Research Article Vol. 6, No. 5 / May 2018 / Photonics Research 479

PHOTONICS Research

Generation of a continuous-variable quadripartite cluster state multiplexed in the spatial domain

Chunxiao Cai,[1,2] Long Ma,[1,2] Juan Li,[1,2] Hui Guo,[1,2] Kui Liu,[1,2] Hengxin Sun,[1,2] Rongguo Yang,[1,2] and Jiangrui Gao[1,2,*]

[1]State Key Laboratory of Quantum Optics and Quantum Optics Devices, Institute of Opto-Electronics, Shanxi University, Taiyuan 030006, China
[2]Collaborative Innovation Center of Extreme Optics, Shanxi University, Taiyuan 030006, China
*Corresponding author: jrgao@sxu.edu.cn

Received 25 January 2018; revised 16 March 2018; accepted 26 March 2018; posted 28 March 2018 (Doc. ID 320573); published 26 April 2018

As a highly entangled quantum network, the cluster state has the potential for greater information capacity and use in measurement-based quantum computation. Here, we report generating a continuous-variable quadripartite "square" cluster state of multiplexing orthogonal spatial modes in a single optical parametric amplifier (OPA), and further improve the quality of entanglement by optimizing the pump profile. We produce multimode entanglement of two first-order Hermite–Gauss modes within one beam in a single multimode OPA and transform it into a cluster state by phase correction. Furthermore, the pump-profile dependence of the entanglement of this state is explored. Compared with fundamental mode pumping, an enhancement of approximately 33% is achieved using the suitable pump-profile mode. Our approach is potentially scalable to multimode entanglement in the spatial domain. Such spatial cluster states may contribute to future schemes in spatial quantum information processing.

OCIS codes: (190.4410) Nonlinear optics, parametric processes; (270.6570) Squeezed states.

https://doi.org/10.1364/PRJ.6.000479

1. INTRODUCTION

Multipartite entanglement is an essential physical resource enabling more complex processing. With its use, the fundamental quantum properties of light have been examined and various quantum-information tasks, such as quantum computation [1,2], quantum error correction [3], and quantum communication [4,5], have been successfully implemented. In recent years, a special type of multipartite entangled state, the cluster state, has attracted attention. Being highly entangled, the cluster state maintains an entanglement structure that is robust to local measurements [6] and can be used for measurement-based quantum computation [1,2,7–11].

There have been numerous demonstrations of cluster states, including the generation of four-mode [12,13] and eight-mode [14] cluster states. However, in using many cavities and separate beams to build the quantum state, the schemes require complex layouts. Very recently, though, a novel and potentially scalable method was proposed to encode deterministically quantum modes propagating within one beam, enabling each quantum mode to be manipulated by the same optical components, and cluster states of an arbitrary size to be generated using a limited and fixed optical setup [15–27]. Previous attempts to create cluster states within one beam have been exploited with orthogonal quantum modes in the frequency domain [15–17] and in the time domain [18–21] by encoding each mode at different times. To date, an ultra-large-scale entangled state consisting of more than 10000 entangled wave packets of light has been experimentally demonstrated [20]. In the spatial domain, entanglement between co-propagating modes in one beam has been demonstrated previously [22], and a cluster state was also created by defining quantum modes to be combinations of different spatial regions of one beam [23]. Yet, to the best of our knowledge, there has been no report on cluster-state generation using different spatial modes on the basis of Hermite–Gaussian (HG) modes and Laguerre–Gaussian (LG) modes. Spatial multimode entanglement in a single multimode optical parametric amplifier (OPA) has been explored [24,25], with the generation of continuous-variable (CV) hyperentanglement [25,26] and spatial quadripartite Greenberger–Horne–Zeilinger (GHZ) entanglement [27] being accomplished.

In this paper, we describe our proposal and demonstration in experiments of spatial-mode quadripartite cluster-state generation in a single OPA operating in multimode. We further enhance the nonlinear efficiency to improve the entanglement by selecting a suitable pump-profile mode. These spatial domain explorations are expected to advance both theory and experimentation on spatial-mode one-way quantum computation.

2. THEORETICAL DESCRIPTION

To create the multipart cluster state, multimode entangled beams are prepared first. We employ the multimode OPA model of Refs. [25,26], which performs multiplexing in the spatial domain and generates hyperentanglement of the polarization and orbital angular momentum (OAM) modes. In the interaction picture, the interaction Hamiltonian of the system is given by [25,26]

$$H_{\text{int}} = i\hbar\chi\sum_{k}(\hat{a}_p\hat{a}^{i\dagger}_{+1}\hat{a}^{s\dagger}_{-1} + \hat{a}_p\hat{a}^{i\dagger}_{-1}\hat{a}^{s\dagger}_{+1} + \text{h.c}), \tag{1}$$

where $\hat{a}_p$ and $\hat{a}^j_l$ denote the bosonic annihilation operators for the pump and fundamental fields, respectively, superscripts j ($j = i, s$) signify signal and idler fields, respectively, and subscripts $l = \pm 1$ index the quantum number of the OAM modes LG^1_0 and LG^{-1}_0; parameter χ denotes the nonlinear coupling strength, which depends on, e.g., the cavity parameters and spatial overlap between the pump and down-conversion fields [28,29]. From the interaction Hamiltonian, Eq. (1), the down-converted signal and idler photons are produced in two OAM modes, LG^1_0 and LG^{-1}_0. By performing a simple-basis transformation from the LG modes to the HG modes, the generated down-converted signal and idler beams also produce four HG modes, HG^i_{01}, HG^s_{01}, HG^i_{10}, and HG^s_{10}. In the following, we use the HG mode basis and rewrite H_{int} as

$$H_{\text{int}} = i\hbar\chi\sum_{k}(\hat{a}_p\hat{a}^{i\dagger}_{10}\hat{a}^{s\dagger}_{10} + \hat{a}_p\hat{a}^{i\dagger}_{01}\hat{a}^{s\dagger}_{01} + \text{h.c}), \tag{2}$$

where subscript 01(10) labels the $\text{HG}_{01(10)}$ mode. The hyperentanglement criteria for the polarization and OAM modes can then also be restated as [25,26]

$$V(\hat{X}^i_{01} + \hat{X}^s_{01}) < 1, \tag{3a}$$

$$V(\hat{Y}^i_{01} - \hat{Y}^s_{01}) < 1, \tag{3b}$$

$$V(\hat{X}^i_{10} + \hat{X}^s_{10}) < 1, \tag{3c}$$

$$V(\hat{Y}^i_{10} - \hat{Y}^s_{10}) < 1, \tag{3d}$$

where $\hat{X}_{01/10} = \hat{a}_{01/10} + \hat{a}^\dagger_{01/10}$ and $\hat{Y}_{01/10} = i(\hat{a}_{01/10} - \hat{a}^\dagger_{01/10})$ are the amplitude and phase quadrature operators of the $\text{HG}_{01/10}$ mode, respectively, and $V(B) = \langle B^2\rangle - \langle B\rangle^2$ denotes the variance of the observable B, which indicates whether both the HG_{01} and HG_{10} modes are entangled independently. After simple transformations, these two-mode entanglements are further transformed into a spatial cluster state [Fig. 1(a)]. Performing the transformation U introduces only a $\frac{\pi}{2}$-phase shift in the two signal fields of the entangled output beam, resulting in $\hat{a}^s_{01} \to i\hat{a}^s_{01}$ and $\hat{a}^s_{10} \to i\hat{a}^s_{10}$. Then, by coupling the two modes as $\hat{a}^s_{135^\circ} = (i\hat{a}^s_{01} + i\hat{a}^s_{10})/\sqrt{2}$ and $\hat{a}^s_{45^\circ} = (i\hat{a}^s_{01} - i\hat{a}^s_{10})/\sqrt{2}$, the quadrature transformation relation becomes

$$\hat{X}^s_{01} = (\hat{Y}^s_{135^\circ} + \hat{Y}^s_{45^\circ})/\sqrt{2}, \tag{4a}$$

$$\hat{Y}^s_{01} = -(\hat{X}^s_{135^\circ} + \hat{X}^s_{45^\circ})/\sqrt{2}, \tag{4b}$$

$$\hat{X}^s_{10} = (\hat{Y}^s_{135^\circ} - \hat{Y}^s_{45^\circ})/\sqrt{2}, \tag{4c}$$

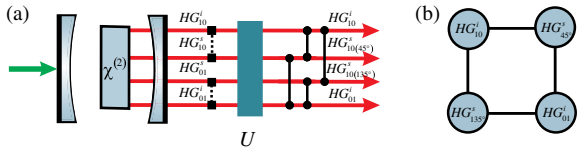

Fig. 1. Schematic of the underlying principle involved in generating the CV quadripartite spatial-mode Gaussian cluster state. (a) Pump laser drives the multimode OPA to produce entanglement of two spatial modes, HG_{01} and HG_{10}, within one beam. By performing the transformation U, the multimode entanglement is transformed into a cluster state containing four spatial orthogonal modes, HG_{01}, HG_{10}, HG_{45°, and HG_{135°. (b) Square representation in the graph-state picture. Each cluster node, corresponding to a spatial mode, is represented by a circle. Neighboring nodes are connected by lines and represent the bipartite entanglement between two spatial modes.

$$\hat{Y}^s_{10} = -(\hat{X}^s_{135^\circ} - \hat{X}^s_{45^\circ})/\sqrt{2}. \tag{4d}$$

Hence, the entanglement criteria, Eq. (3), read

$$V\left(\hat{Y}^i_{01} + \frac{1}{\sqrt{2}}\hat{X}^s_{135^\circ} + \frac{1}{\sqrt{2}}\hat{X}^s_{45^\circ}\right) < 1, \tag{5a}$$

$$V\left(\hat{Y}^i_{10} + \frac{1}{\sqrt{2}}\hat{X}^s_{135^\circ} - \frac{1}{\sqrt{2}}\hat{X}^s_{45^\circ}\right) < 1, \tag{5b}$$

$$V\left(\hat{Y}^s_{45^\circ} + \frac{1}{\sqrt{2}}\hat{X}^i_{01} - \frac{1}{\sqrt{2}}\hat{X}^i_{10}\right) < 1, \tag{5c}$$

$$V\left(\hat{Y}^s_{135^\circ} + \frac{1}{\sqrt{2}}\hat{X}^i_{01} + \frac{1}{\sqrt{2}}\hat{X}^i_{10}\right) < 1, \tag{5d}$$

which satisfy the definition of a CV cluster-state given by [13,30]

$$\hat{Y} - A\hat{X} \to 0, \tag{6}$$

where A is the adjacency matrix, representing the graph of a given CV state. Therefore, the spatial multimode OPA can be used to generate a spatial-mode cluster state. We give the graph-state picture representation [Fig. 1(b)] describing the "square" correlation among the four modes. Each cluster node, corresponding to a spatial mode, is represented by a circle. Neighboring nodes are connected by lines and represent the bipartite entanglement between two spatial modes. Using the quadrature transformation relations, Eq. (4), the entanglement criteria, Eq. (5), can be restated as phase quadrature variances of the HG modes, HG_{01}, HG_{10}, HG_{45° and HG_{135°:

$$V(\hat{Y}^i_{01} - \hat{Y}^s_{01}) < 1, \tag{7a}$$

$$V(\hat{Y}^i_{10} - \hat{Y}^s_{10}) < 1, \tag{7b}$$

$$V(\hat{Y}^i_{45^\circ} - \hat{Y}^s_{45^\circ}) < 1, \tag{7c}$$

$$V(\hat{Y}^i_{135^\circ} - \hat{Y}^s_{135^\circ}) < 1. \tag{7d}$$

Clearly, the spatial-mode cluster state, Eq. (5), can be characterized using phase quadrature correlations for all four modes and is easy to measure in experiments.

Essentially, the spatial-state generation in optical parametric oscillator (OPO) depends closely on the transverse profile matching between pump mode and generated modes [26,27]. Different pump-mode profiles result in different nonlinear efficiencies and different pump thresholds, thus leading to different degrees of entanglement. More importantly, maximum entanglement can be obtained only with an optimal pump profile.

For the spatial cluster state, which generates HG_{01} and HG_{10} down-conversion modes simultaneously, the transverse distribution of the pump mode is expressed as $\nu^p(\vec{r}) = \Sigma_{n=0}^{\infty} c_n[\nu_{n0}(\vec{r}) + \nu_{0n}(\vec{r})]$ [28,29], where ν_{n0} and ν_{0n} denote the transverse profiles of the HG_{n0} and HG_{0n} modes, respectively, and c_n is the corresponding coefficient. We can calculate the pump profile based on the definition of the coupling coefficient, which describes the spatial overlap between the pump and the two down-conversion modes in the transverse plane, and is defined by

$$\Gamma = \int_{-\infty}^{+\infty} \frac{\nu^p(\vec{r})\mu^s(\vec{r})\mu^i(\vec{r})}{\alpha} \mathrm{d}\vec{r}, \tag{8}$$

where $\mu^s(\vec{r})$ and $\mu^i(\vec{r})$ are the transverse distributions of the signal and idler modes, respectively, and α, the normalization coefficient of the squared signal, is defined as $\alpha^2 = \int_{-\infty}^{+\infty} \mu^4(\vec{r})\mathrm{d}\vec{r}$. For the $HG_{01/10}$ down-conversion mode, only two nonzero overlapping coefficients result from Eq. (8):

$$\Gamma_{00} = \int_{-\infty}^{+\infty} \frac{\nu_{00}(\vec{r})\mu_{01/10}^2(\vec{r})}{\sqrt{\int_{-\infty}^{+\infty} \mu_{01/10}^4(\vec{r})\mathrm{d}\vec{r}}} \mathrm{d}\vec{r} = \sqrt{\frac{1}{3}}, \tag{9a}$$

$$\Gamma_{02/20} = \int_{-\infty}^{+\infty} \frac{\nu_{02/20}(\vec{r})\mu_{01/10}^2(\vec{r})}{\sqrt{\int_{-\infty}^{+\infty} \mu_{01/10}^4(\vec{r})\mathrm{d}\vec{r}}} \mathrm{d}\vec{r} = \sqrt{\frac{2}{3}}, \tag{9b}$$

for which $\Gamma_{00}^2 + \Gamma_{02/20}^2 = 1$ holds, and subscripts 00 and 02/20 of Γ indicate the transverse distribution of the pump mode HG_{00} and $HG_{02/20}$. Hence, the pump-mode profile for $HG_{01/10}$ down-conversion modes can be HG_{00} and $HG_{02/20}$ modes, and the optimal pump mode is the superposition of the HG_{00} and $HG_{02/20}$ modes, of which the $HG_{02/20}$ accounts for two thirds. The only pump-mode profiles for the spatial cluster state are therefore the HG_{00} and the superposition of HG_{02} and HG_{20} modes, where the superposition mode is equal to LG_1^0 mode. The optimal pump profile is the superposition of the HG_{00} and LG_1^0 modes, of which LG_1^0 accounts for two thirds, and we have $\Gamma_{\mathrm{opt}} = 1$. When pumping in the HG_{00}, LG_1^0, and the optimal profile, the system increases its threshold inversely proportional to the square of the overlap coefficient. In 2017, Pereira *et al.* also found similar phenomena in type II second-harmonic generation, which is the reverse process of OPA [31]. By mixing opposite topological charges +1 and −1, they obtained the superposition between HG_{00} and LG_1^0 modes. Moreover, the generation of higher radial orders was demonstrated when higher opposite charges were mixed in the crystal. This can motivate future investigations with higher radial orders and higher topological charges in the OPO as well.

Although the spatial profile of an ideal pump is the superposition of HG_{00} and LG_1^0 modes, the efficiency of the LG_1^0 mode pump is two times that of HG_{00}. We can almost achieve optimal entanglement by simply using only the LG_1^0 pump mode.

3. EXPERIMENTAL SETUP AND RESULTS

The experimental setup (Fig. 2) entails entanglement source generation, LG pump generation, and balanced homodyne detection. Our OPA cavity is formed by the rear surface of a type-II phase-matched potassium titanyl phosphate (KTP) crystal (KTP1) and an external mirror (radius of curvature is 50 mm, and $R = 95\%$ at 1080 nm). An additional KTP crystal (KTP2) of identical size is placed with the z axis orthogonal to KTP1, to compensate the Gouy phase difference induced by astigmatism [32], and a 1080-nm half-wave plate oriented at 22.5° is inserted between the two crystals, so that the HG_{10} and HG_{01} modes of different polarizations resonate simultaneously in the OPA. This degeneracy is further optimized by individually controlling the temperature of the two KTP crystals. The length of the cavity is approximately 57.8 mm, resulting in a free spectral range of about 2.6 GHz and a finesse of 91 at 1080 nm. The cavity has a waist of 40 μm at 1080 nm and 28.5 μm at 540 nm. The cavity loss is approximately 1.44%.

A 45°-polarized HG_{01} weak field at 1080 nm is injected into the OPA cavity as a seed beam, and a fundamental mode or LG_1^0 light beam operating at 540 nm is used as the pump field to drive the OPA. Here, we achieve the LG_1^0-mode by converting the HG_{11}-mode with a HG_{11}–LG_1^0 mode converter [33], where the HG_{11}-mode is achieved by tailoring the fundamental mode with a four-quadrant phase mask and a filtering cavity. When operated in the de-amplification regime, the OPA produces simultaneously a bright entangled HG_{01} beam and a vacuum-entangled HG_{10} beam in the cavity. The output multimode entangled beam then passes through a quarter-wave plate with its fast axis aligned with the s-polarization axis of

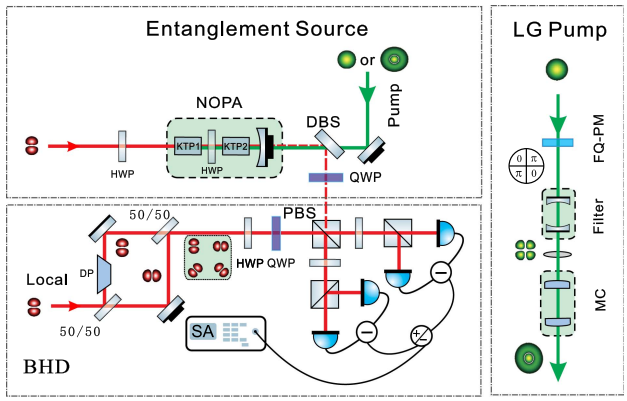

Fig. 2. Experimental layout for the generation and characterization of the spatial-mode cluster state. Entanglement is generated using a multimode OPA and measured by BHD detection with spatial tailored local oscillators. LG_1^0 pump reconstruction is shown in the right panel. NOPA: nondegenerate optical parametric amplifier; LO: local oscillator; DBS: dichroic beam splitter; PBS: polarization beam splitter; HWP: half-wavelength plate; QWP: quarter-wave plate; BHD: balanced homodyne detection; DP: Dove prism; SA: spectrum analyzer; FQ-PM: four-quadrant phase mask; MC: HG_{11}–LG_1^0 mode converter.

beam splitter output to induce a phase shift in the s-polarization with respect to p-polarization. Then the beam is analyzed using the balanced homodyne detection systems with the local oscillator operating in the HG_{01}, HG_{10}, $HG_{45°}$, and $HG_{135°}$ modes, respectively. We spatially tailor the measurement basis using a Mach–Zehnder interferometer with a Dove prism in one arm to convert a HG_{01} mode into HG_{10} mode. This arrangement can be used to generate an arbitrary first-order mode when both the beam splitting ratio and the relative phase between two arms can be controlled. Measurements are conducted with the relative phase between the local oscillator and the signal beam locked to $\frac{\pi}{2}$, so that the phase quadrature variances can be obtained.

We show the measured correlation variance spectra (Figs. 3 and 4) for the range of 1–6 MHz obtained using Eq. (7) with the HG_{00}- and LG_1^0-mode pump beams, respectively. Traces (2) correspond to the shot noise limit (SNL), which is obtained by blocking the signal beam, and traces (1) and (3) are the correlation variance and anti-correlation variance, respectively. In both figures, (a)–(d) correspond to the phase quadrature correlations for the HG_{01}, HG_{10}, $HG_{45°}$, and $HG_{135°}$ modes. When pumping with the HG_{00}-mode beam (Fig. 3), we obtained the correlation variances with mean values of 2.20 ± 0.12 dB, 2.30 ± 0.12 dB, 1.93 ± 0.13 dB, and 2.15 ± 0.14 dB, respectively, over the entire frequency range. As the analyzing frequency increases, the traces of the anti-correlation variance diminish because of the limited bandwidth of the electron gain of the detectors. The parameter settings of the spectrum analyzer are 300 kHz and 390 Hz for the resolution and video bandwidths, respectively. From the well-established inseparability criteria inequalities for the cluster-state entanglement, Eq. (7), we obtain

$$V(\hat{Y}^i_{01} - \hat{Y}^s_{01}) = 0.62 \pm 0.02 < 1, \quad \textbf{(10a)}$$

$$V(\hat{Y}^i_{10} - \hat{Y}^s_{10}) = 0.59 \pm 0.02 < 1, \quad \textbf{(10b)}$$

$$V(\hat{Y}^i_{45°} - \hat{Y}^s_{45°}) = 0.64 \pm 0.02 < 1, \quad \textbf{(10c)}$$

$$V(\hat{Y}^i_{135°} - \hat{Y}^s_{135°}) = 0.61 \pm 0.02 < 1. \quad \textbf{(10d)}$$

The LG_1^0-mode as a pump provides better efficiency. All four correlation variances show improvements (Fig. 4); mean values of 3.15 ± 0.11 dB, 3.63 ± 0.12 dB, 3.20 ± 0.12 dB, and 3.32 ± 0.14 dB were obtained. Compared with HG_{00} pumping, an enhancement of approximately 33% is achieved. Their corresponding values for non-separability (Fig. 5) are also improved:

$$V(\hat{Y}^i_{01} - \hat{Y}^s_{01}) = 0.48 \pm 0.02 < 1, \quad \textbf{(11a)}$$

$$V(\hat{Y}^i_{10} - \hat{Y}^s_{10}) = 0.43 \pm 0.02 < 1, \quad \textbf{(11b)}$$

$$V(\hat{Y}^i_{45°} - \hat{Y}^s_{45°}) = 0.48 \pm 0.02 < 1, \quad \textbf{(11c)}$$

$$V(\hat{Y}^i_{135°} - \hat{Y}^s_{135°}) = 0.47 \pm 0.02 < 1. \quad \textbf{(11d)}$$

The measured inseparabilities and correlation are affected by various inefficiencies in the experiment. We estimate the total detection efficiency to be $\eta_{\text{total}} = \eta_{\text{prop}}\eta_{\text{phot}}\eta_{\text{hd}}$, where $\eta_{\text{prop}} = 0.96 \pm 0.02$, $\eta_{\text{phot}} = 0.92 \pm 0.02$, and $\eta_{\text{hd}} = 0.96 \pm 0.02$ are respective of the measured propagation efficiency, photodiode (ETX500) efficiency, and spatial overlap efficiency in the homodyne detector. Thus, the inferred inseparability values are: $V(\hat{Y}^i_{01} - \hat{Y}^s_{01}) = 0.36 \pm 0.02$, $V(\hat{Y}^i_{10} - \hat{Y}^s_{10}) = 0.30 \pm 0.02$, $V(\hat{Y}^i_{45°} - \hat{Y}^s_{45°}) = 0.36 \pm 0.02$, and $V(\hat{Y}^i_{135°} - \hat{Y}^s_{135°}) = 0.35 \pm 0.02$, and the inferred correlation variances (Fig. 4) are: -4.44 ± 0.11 dB, -5.23 ± 0.12 dB, -4.44 ± 0.12 dB, and -4.56 ± 0.14 dB.

In addition to the inefficiencies in measurement discussed above, cavity loss resulting from the non-optimal dielectric

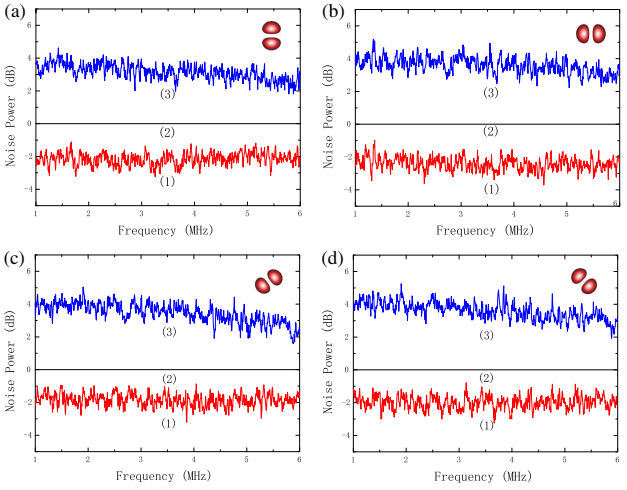

Fig. 3. Measured quantum correlations of the cluster state in the mode basis (a) HG_{01}, (b) HG_{10}, (c) $HG_{45°}$, and (d) $HG_{135°}$ using the fundamental mode pump. Trace (2) is the shot noise limit (SNL), and traces (1) and (3) are the correlation variance and anti-correlation variance, respectively, normalized to SNL. Measurement settings: resolution bandwidth 300 kHz, video bandwidth 390 Hz.

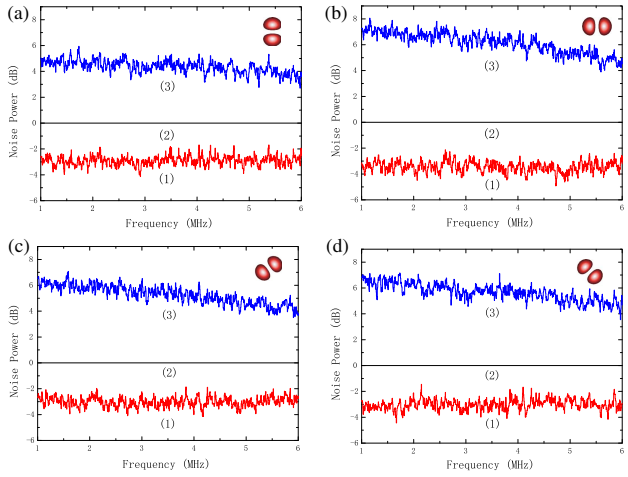

Fig. 4. Enhanced entanglement for the (a) HG_{01}, (b) HG_{10}, (c) $HG_{45°}$, and (d) $HG_{135°}$ modes with LG_1^0 pumping. Trace (2) is SNL; traces (1) and (3) are the correlation variances normalized to SNL. Measurement settings: resolution bandwidth 300 kHz, video bandwidth 390 Hz.

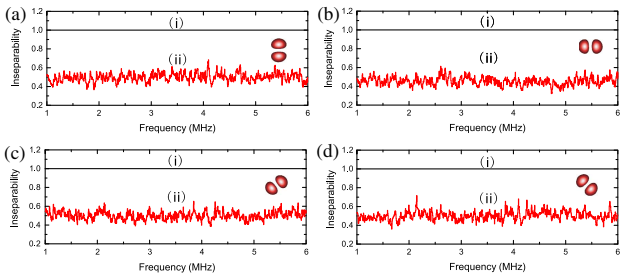

Fig. 5. Experimental measurement of inseparability for the (a) HG_{01}, (b) HG_{10}, (c) $HG_{45°}$, and (d) $HG_{135°}$ modes with LG_1^0 pumping. Values below unity indicate entanglement.

coatings on optical elements is also a main factor that limits the quality of entanglement. Also, extra noise in the laser, imperfect phase locking, and so on, will also degrade the correlation. The entanglement can be improved by optimizing the experimental setup for future applications.

4. CONCLUSION

We have experimentally demonstrated the CV quadripartite spatial-mode "square" cluster-state generation by multiplexing orthogonal spatial modes within one beam in a single multimode OPA. The degree of freedom is extended in the spatial mode domain, and the generation setup is much simpler with only one OPA cavity. Realizing a compact Gaussian quantum computation using a multi-pixel detector or charge coupled device (CCD) [34] looks promising. Using this infinite spatial basis within a single beam, and the possible manipulation of the modes, makes it a practical contender for spatial multimode quantum communication systems. Furthermore, we explored the dependence of entanglement of the spatial cluster state on the pump profile, and demonstrated the enhancement for the spatial cluster state with a LG_1^0 pump profile. The approach described can be extended to other more complex graph states if a suitable pump profile is used [35,36].

Funding. National Natural Science Foundation of China (NSFC) (91536222, 11674205); Ministry of Science and Technology of the People's Republic of China (MOST) (2016YFA0301404); Program for the Outstanding Innovative Team of Higher Learning Institution of Shanxi and Shanxi "1331 Project."

REFERENCES

1. R. Raussendorf and H. J. Briegel, "A one-way quantum computer," Phys. Rev. Lett. **86**, 5188–5191 (2001).
2. R. N. Alexander, P. Wang, N. Sridhar, M. Chen, O. Pfister, and N. C. Menicucci, "One-way quantum computing with arbitrarily large time-frequency continuous-variable cluster states from a single optical parametric oscillator," Phys. Rev. A **94**, 032327 (2016).
3. T. Aoki, G. Takahashi, T. Kajiya, J. Yoshikawa, S. L. Braunstein, P. van Loock, and A. Furusawa, "Quantum error correction beyond qubits," Nat. Phys. **5**, 541–546 (2009).
4. X. L. Wang, X. D. Cai, Z. E. Su, M. C. Chen, D. Wu, L. Li, N. L. Liu, C. Y. Lu, and J. W. Pan, "Quantum teleportation of multiple degrees of freedom of a single photon," Nature **518**, 516–519 (2015).
5. W. McCutcheon, A. Pappa, B. A. Bell, A. McMillan, A. Chailloux, T. Lawson, M. Mafu, D. Markham, E. Diamanti, I. Kerenidis, J. G. Rarity, and M. S. Tame, "Experimental verification of multipartite entanglement in quantum networks," Nat. Commun. **7**, 13251 (2016).
6. H. J. Briegel and R. Raussendorf, "Persistent entanglement in arrays of interacting particles," Phys. Rev. Lett. **86**, 910–913 (2001).
7. J. Zhang and S. L. Braunstein, "Continuous-variable Gaussian analog of cluster states," Phys. Rev. A **73**, 032318 (2006).
8. N. C. Menicucci, P. van Loock, M. Gu, C. Weedbrook, T. C. Ralph, and M. A. Nielsen, "Universal quantum computation with continuous-variable cluster states," Phys. Rev. Lett. **97**, 110501 (2006).
9. P. Walther, K. J. Resch, T. Rudolph, E. Schenck, H. Weinfurter, V. Vedral, M. Aspelmeyer, and A. Zeilinger, "Experimental one-way quantum computing," Nature **434**, 169–176 (2005).
10. Y. Tokunaga, S. Kuwashiro, T. Yamamoto, M. Koashi, and N. Imoto, "Generation of high-fidelity four-photon cluster state and quantum-domain demonstration of one-way quantum computing," Phys. Rev. Lett. **100**, 210501 (2008).
11. R. Ukai, N. Iwata, Y. Shimokawa, S. Armstrong, A. Politi, J. Yoshikawa, P. V. Loock, and A. Furusawa, "Demonstration of unconditional one-way quantum computations for continuous variables," Phys. Rev. Lett. **106**, 240504 (2011).
12. X. Su, A. Tan, X. Jia, J. Zhang, C. Xie, and K. Peng, "Experimental preparation of quadripartite cluster and Greenberger-Horne-Zeilinger entangled states for continuous variables," Phys. Rev. Lett. **98**, 070502 (2007).
13. M. Yukawa, R. Ukai, P. van Loock, and A. Furusawa, "Experimental generation of four-mode continuous-variable cluster states," Phys. Rev. A **78**, 012301 (2008).
14. X. Su, Y. Zhao, S. Hao, X. Jia, C. Xie, and K. Peng, "Experimental preparation of eight-partite cluster state forphotonic qumodes," Opt. Lett. **37**, 5178–5180 (2012).
15. M. Pysher, Y. Miwa, R. Shahrokhshahi, R. Bloomer, and O. Pfister, "Parallel generation of quadripartite cluster entanglement in the optical frequency comb," Phys. Rev. Lett. **107**, 030505 (2011).
16. J. Roslund, R. Medeiros de Arajo, S. Jiang, C. Fabre, and N. Treps, "Wavelength-multiplexed quantum networks with ultrafast frequency combs," Nat. Photonics **8**, 109–112 (2014).
17. N. C. Menicucci, S. T. Flammia, and O. Pfister, "One-way quantum computing in the optical frequency comb," Phys. Rev. Lett. **101**, 130501 (2008).
18. N. C. Menicucci, "Temporal-mode continuous-variable cluster states using linear optics," Phys. Rev. A **83**, 062314 (2011).
19. N. C. Menicucci, X. Ma, and T. C. Ralph, "Arbitrarily large continuous-variable cluster states from a single quantum nondemolition gate," Phys. Rev. Lett. **104**, 250503 (2010).
20. S. Yokoyama, R. Ukai, S. C. Armstrong, C. Sornphiphatphong, T. Kaji, S. Suzuki, J. Yoshikawa, H. Yonezawa, N. C. Menicucci, and A. Furusawa, "Ultra-large-scale continuous-variable cluster states multiplexed in the time domain," Nat. Photonics **7**, 982–986 (2013).
21. J. Yoshikawa, S. Yokoyama, T. Kaji, C. Sornphiphatphong, Y. Shiozawa, K. Makino, and A. Furusawa, "Generation of one-million-mode continuous-variable cluster state by unlimited time-domain multiplexing," APL Photon. **1**, 060801 (2016).
22. J. Janousek, K. Wagner, J. F. Morizur, N. Treps, P. K. Lam, C. C. Harb, and H. A. Bachor, "Optical entanglement of co-propagating modes," Nat. Photonics **3**, 399–402 (2009).
23. S. Armstrong, J.-F. Morizur, J. Janousek, B. Hage, N. Treps, P. K. Lam, and H.-A. Bachor, "Programmable multimode quantum networks," Nat. Commun. **3**, 1026 (2012).
24. S. L. W. Midgley, A. S. Bradley, O. Pfister, and M. K. Olsen, "Quadripartite continuous-variable entanglement via quadruply concurrent down-conversion," Phys. Rev. A **81**, 063834 (2010).
25. B. dos Santos, K. Dechoum, and A. Khoury, "Continuous-variable hyperentanglement in a parametric oscillator with orbital angular momentum," Phys. Rev. Lett. **103**, 230503 (2009).
26. K. Liu, J. Guo, C. Cai, S. Guo, and J. Gao, "Experimental generation of continuous-variable hyperentanglement in an optical parametric oscillator," Phys. Rev. Lett. **113**, 170501 (2014).

27. K. Liu, J. Guo, C. Cai, J. Zhang, and J. Gao, "Direct generation of spatial quadripartite continuous variable entanglement in an optical parametric oscillator," Opt. Lett. **41**, 5178–5181 (2016).
28. J. Guo, C. Cai, L. Ma, K. Liu, H. Sun, and J. Gao, "Higher order mode entanglement in a type II optical parametric oscillator," Opt. Express **25**, 4985–4993 (2017).
29. M. Lassen, V. Delaubert, C. Harb, P. K. Lam, N. Treps, and H. A. Bachor, "Generation of squeezing in higher order Hermite-Gaussian modes with an optical parametric amplifier," J. Eur. Opt. Soc. Rapid Publ. **1**, 06003 (2006).
30. S. L. W. Midgley, M. K. Olsen, A. S. Bradley, and O. Pfister, "Analysis of a continuous-variable quadripartite cluster state from a single optical parametric oscillator," Phys. Rev. A **82**, 053826 (2010).
31. L. J. Pereira, W. T. Buono, D. S. Tasca, K. Dechoum, and A. Z. Khoury, "Orbital-angular-momentum mixing in type-II second-harmonic generation," Phys. Rev. A **96**, 053856 (2017).
32. M. Martinelli, J. A. O. Huguenin, P. Nussenzveig, and A. Z. Khoury, "Orbital angular momentum exchange in an optical parametric oscillator," Phys. Rev. A **70**, 013812 (2004).
33. M. W. Beijersbergen, L. Allen, H. van der Veen, and J. P. Woerdman, "Astigmatic laser mode converters and transfer of orbital angular momentum," Opt. Commun. **96**, 123–132 (1993).
34. G. Ferrini, J. P. Gazeau, T. Coudreau, C. Fabre, and N. Treps, "Compact Gaussian quantum computation by multi-pixel homodyne detection," New J. Phys. **15**, 093015 (2013).
35. J. Zhang, J. J. Wang, R. G. Yang, K. Liu, and J. R. Gao, "Large-scale continuous-variable dual-rail cluster entangled state based on spatial mode comb," Opt. Express **25**, 27172–27181 (2017).
36. R. C. Pooser and J. Jing, "Continuous variable cluster state generation over the optical spatial mode comb," Phys. Rev. A **90**, 043841 (2014).